Preliminary Simulation Study of Flow Field Around a Spark Plug Under Ambient and Engine Conditions

Navjot Sandhu, Shouvik Dev, Divyanshu Purohit, Zhenyi Yang, Ming Zheng(✉), and David Ting

Department of Mechanical, Automotive and Materials Engineering, University of Windsor, 401 Sunset Ave, Windsor, ON, Canada
mzheng@uwindsor.ca

Abstract. Sustainable transportation solutions for the future would require advanced powertrains which can meet the goals of emission and fuel consumption reduction. One option could be high-efficiency spark ignition (SI) internal combustion engines using conventional or renewable fuels. Such SI engines in the future may operate under lean conditions at which the air is in excess with respect to the fuel. Typically, ignition and complete combustion of such a lean mixture of air and fuel is a challenge owing to the reduced charge reactivity. One solution is to enhance the in-cylinder charge motion to increase the flame velocity. However, this charge motion can affect the initial spark breakdown and the consequent flame kernel development. Therefore, in order to estimate the flow field around the spark plug, a simulation study is undertaken. The simulations are performed using Converge™ three-dimensional simulation suite (version 2.3). ANSYS EnSight (version 10.1) is used for post-processing of the simulation data. Two types of flow fields are simulated. The first flow field simulates a cross-flow of air across the electrode gap of a conventional J-type spark plug under ambient pressure. The flow upstream of the plug is laminar, and the flow velocity is varied. This part of the study is used to determine the effect of the spark plug geometry on the flow. The second condition simulates the in-cylinder flow field of a two-valve, single-cylinder engine. The intake air flow rate is the main variable. The numerical estimation of the flow velocity and the turbulence around the spark gap are correlated with the experimental results. Preliminary results indicate that the spark plug can generate turbulence in its wake under steady flow conditions and the vorticity magnitudes can be correlated to the electrical parameters. In the engine, the flow field in and near the spark gap may not correlate with the bulk air motion.

1 Introduction

The quest for sustainable transportation solutions has prompted research and development into advanced powertrains that can meet or exceed standards for emissions and fuel efficiency. Such advanced powertrains may continue to use spark ignition (SI) internal combustion engines with conventional or low-carbon footprint alternative fuels [1–3]. Since gasoline-fueled SI engines dominate the international passenger

A. Vasel and D. S.-K. Ting (Eds.): EAS 2018, SPE, pp. 34–54, 2019.
https://doi.org/10.1007/978-3-030-00105-6_3

vehicle market, improvements in efficiency can make a significant impact on energy security and environment [4]. Lean and diluted combustion have been proposed as two effective methods for increasing the efficiency of SI engines and decreasing the engine-out emissions [5, 6]. Conventional SI engines typically operate under stoichiometric conditions with all the intake air being utilized for complete combustion of the fuel. For lean combustion, intake air supply is more than what is required for complete combustion of the fuel. For diluted combustion, the fresh intake air is mixed with the recirculated exhaust gas (process referred to as exhaust gas recirculation (EGR)) before this mixture is introduced into the cylinder. In addition to reducing nitrogen oxides (NOx) emissions due to lower flame temperature, EGR also has a positive impact on fuel consumption due to reduced throttling losses [7–10]. However, operating the SI engine under lean conditions or with EGR dilution reduces the reactivity of the fuel–air mixture which could lead to poor ignitability. This in turn would limit the level of dilution due to the onset of misfire [5]. Another adverse consequence of lean or diluted combustion is the lower flame speed [11]. The lower flame speed could reduce the fuel efficiency due to incomplete combustion of the fuel–air mixture.

One of the strategies to counter these effects and accelerate the flame velocity is to increase turbulence inside the cylinder by enhancing the motion of the fuel–air mixture. It has been established through experimental and numerical studies that the fluid flow characteristics of the in-cylinder mixture affect the combustion process at a fundamental level [12]. Faster flame speed in an SI engine can help in boosting the thermal efficiency and reducing the NOx emissions by extending the stable lean burn limit, thus making very diluted fuel–air mixtures viable for engine operation [13]. However, this increased in-cylinder turbulence can have adverse effects on the initial spark breakdown and the subsequent flame kernel development process. Excess turbulence can also lead to extinguishment of the flame. Instability in the early stages of combustion can significantly contribute toward cyclic variations in the engine operation [14–16]. Studies have shown that the plasma channel in the spark gap tends to stretch and follow the flow field [17, 18]. While this stretch helps in increasing the total surface area of the spark plasma, the energy density of the spark channel can diminish to a large extent, depending on the flow velocity. Consequently, the air–fuel mixture can either fail to ignite entirely or the initial flame kernel can form and then later be extinguished due to the inability to sustain the combustion [17]. In order to mitigate the negative effects of turbulence on the formation and sustainability of the spark channel, it is imperative to understand the flow field around the spark plug during ignition timing. Eventually, this flow field may be controlled to optimize the combustion event.

There has been a substantial amount of research on the effects of air motion on the spark ignition using constant volume combustion chambers as well as research engine platforms [16–22]. Sayama et al. studied the spark ignition and early flame development at lean air–fuel ratios of 20–30 under high-velocity flow conditions of $\sim$65 m/s at the spark gap in a swirl chamber. The authors found that the spark channels stretched downstream of the spark plug to follow the flow field and frequent restrikes or short circuits were apparent [17]. The findings also demonstrated that the degree of dilution had a significant effect on flame development and sustainability following the initial spark event. Aleiferis et al. used a single-cylinder optical research engine with a pent-roof combustion chamber and variable valve actuation to study the effect of flow

characteristics and spark plug orientation on early flame kernel development and cyclic variations [18]. Direct imaging demonstrated the effect of orientation of spark plug with respect to the flow on the spark channel stretch and the subsequent cyclic variations in the flame development. Additionally, they observed that the flame kernel shape was never spherical and the aspect ratio indicated the dominant effect of large-scale turbulence features. Johansson investigated the effect of several important parameters including flow field, gas composition, and temperature on the early combustion [16]. He concluded that substantial amount of fluctuations during early combustion at high engine load conditions can be attributed to the flow field turbulence and the mixture composition near the spark plug.

Arcoumanis and Bae studied ignition of propane–air mixtures using laser Doppler velocimetry (LDV) and shadowgraphy in a constant volume combustion vessel [19]. They reported that the orientation of spark plug with respect to the mean flow had greater effect at higher velocity as compared to low-velocity cases. Plug orientation with ground electrode downstream of the flow had the highest flame velocity, whereas the upstream ground electrode configuration dampened the effect of turbulence and slowed down the flame speed possibly due to shrouding of the flow by the ground electrode. Ballal and Lefebvre investigated the effect of air flow on electrical parameters of spark ignition in a specially designed wind tunnel at different pressures and velocities of up to 100 m/s [20]. Their findings demonstrated that spark duration decreased with increase in velocity, whereas the minimum energy required for successful ignition showed an increasing trend. Yu et al. studied spark discharge affected by directed flow on the spark gap in a constant volume combustion chamber through optical diagnosis and measurement of electrical parameters [21]. The authors observed the stretch of the spark plasma channel underflow with continuous breakage and re-establishment of the channel (termed as restrike process). The frequency of this restrike process increased with increase inflow velocity, thereby highlighting the difficulty in maintaining the spark plasma channel under high flow conditions.

Based on the authors' search, the flow conditions around the spark plug at the time of ignition have a profound effect on the spark discharge and the subsequent formation of the spark flame kernel. Given the difficulty in the ignition of lean or diluted fuel–air mixtures, the importance of the flow structure is of greater significance. Therefore, in the present research, the authors have undertaken a simulation study to estimate the flow field in the vicinity of the spark plug during the spark event. This study is divided into two parts. The first part of the study simulates a simplified condition in which a steady and uniform cross-flow of air is directed across the electrode gap of a conventional J-type spark plug under ambient conditions. The objective is to determine the effect of the spark plug geometry on the flow field around the spark plug. The second part of the study simulates the in-cylinder flow field of a two-valve, single-cylinder engine during the spark timing window. The simulations are performed using Converge^{TM} three-dimensional simulation suite (version 2.3). ANSYS EnSight (version 10.1) is used for post-processing of the simulation data. The flow field is quantified around the spark plug, especially the spark gap, under different throttle openings and engine speeds. The broader objective of this study is to provide the engine operating conditions which could be favorable to initiate the spark discharge.

This paper is organized as follows. The methodology including the engine research platform which is used to validate the in-cylinder flow field model and the details of the CFD simulation parameters are described in the following section. The simulation validation results are presented in the subsequent section followed by the results for the steady cross-flow and the in-cylinder flow field. The final section describes the summary and main conclusions of this research.

2 Research Methodology

2.1 Engine Research Platform

The test engine used in this study was a Yanmar NFD-170, a two-valve single-cylinder stationary diesel engine, which was heavily modified and instrumented for spark ignition research. This included reducing the compression ratio of the diesel engine to 9.2:1 by modifying the piston bowl. The specifications of the engine are summarized in Table 1. The engine was connected to a General Electric® 26G215 direct current (DC) dynamometer. Intake pressure was controlled through an electronic pressure regulator. The intake air flow rate was measured using a ROOTS volumetric flow meter. The spark plug used for ignition was a conventional J-type resistive spark plug with 14 mm metric thread. In-cylinder pressure was recorded using Kistler piezoelectric pressure transducer and was synchronized with the crank position using a crankshaft rotary encoder and camshaft sensor. National Instruments-Data Acquisition (NI-DAQ) card along with the LabVIEW 2010 software package was used to record the pressure data at 0.1-crank angle degree (°CA) resolution. This engine research platform is instrumented for detailed emission measurement. For this study, the engine research platform was only used to determine the motoring pressure traces (no combustion) for validation of the simulated gas exchange process.

Table 1. Engine specifications

Engine	Yanmar NFD-170
Engine type	4-stroke spark ignited
Bore (mm)	102
Stroke (mm)	105
Displacement (cm^3)	858
Connecting rod length (mm)	165
Compression ratio	9.2:1
Intake valve closing (BTDC[a])	135°
Intake valve open interval (CA[b])	229°

[a]Before Top Dead Center
[b]Crank Angle

2.2 CFD Simulation

Two types of flow field were simulated using Converge™ three-dimensional simulation suite. For the first case, a steady and uniform cross-flow of air across the spark gap was

simulated at different flow velocities to investigate the effect of spark plug geometry on the flow field (Fig. 1). A steady-state density-based solver was used. The spark plug was placed in a large volume to ensure that the flow is fully developed before it reaches the spark gap. For the cross-flow case, a constant inlet velocity boundary condition was used. Wall temperature and initial pressure were 298°K and 1 bar, respectively. The base grid size was 4 mm with the fourth level of grid refinement near the spark plug, reducing the grid size in the vicinity of the spark plug to 0.25 mm. The Renormalized Group (RNG) k-ε turbulence model was used to model the turbulence.

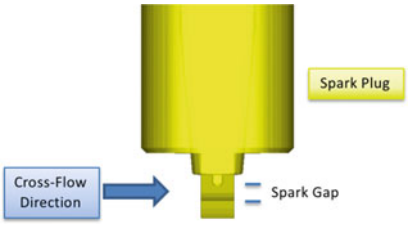

Fig. 1. Spark plug model for cross-flow case

Second case was the engine motoring simulation at different intake mass flow rates and engine speeds. A transient density-based solver was utilized along with the RNG k-ε turbulence model. Since the intake port geometry has a significant influence on the in-cylinder flow [13], the intake port geometry was modeled with high accuracy. To this end, a flexible foam mold cast of the intake port was made and laser scanned. The geometry input for the engine motoring cases is shown in Fig. 2.

The simulation time period extended from 360° BTDC to 100° after TDC. Selective grid refinement was performed to get a balance between computational accuracy and simulation time. Base grid size of 4 mm was used for the model. Third-level grid refinement was performed at the intake valve region during the intake valve event and in the vicinity of the spark plug in the spark discharge window of 100° BTDC to −30° BTDC. Additionally, adaptive mesh refinement (AMR) using velocity was activated in the cylinder region. For the engine motoring case, the intake manifold pressure measurement at 0.1° crank angle resolution was used as a boundary condition for the intake port inflow boundary. The intake and exhaust valve lift profiles were determined experimentally from the test engine and were used as input for the intake and exhaust valve moving boundaries. The wall temperature was 353 K for the boundaries in contact with the in-cylinder gas in accordance with the coolant temperature of the test engine setup. The boundary conditions are listed in Table 2. To account for the crevice volume effect, the effective compression ratio was adjusted to 8.7 for all flow conditions. ANSYS EnSight 10.1 was used to post-process the simulation results data and visualize the flow. The next section describes the validation results.

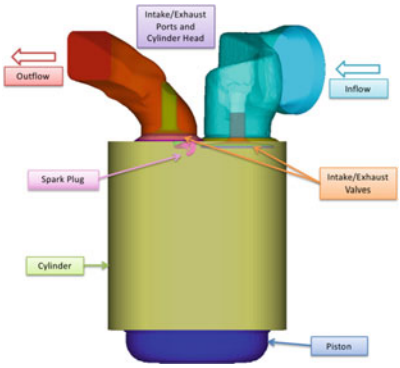

Fig. 2. Geometric model for Engine motoring

Table 2. Engine model boundary conditions

Boundary	Boundary condition
Intake/exhaust port	No-slip stationary wall
Cylinder head	No-slip stationary wall
Inflow	Manifold pressure
Outflow	Zero-gradient pressure
Intake/exhaust valves	No-slip moving wall
Spark plug	No-slip stationary wall
Cylinder	No-slip stationary wall
Piston	No-slip moving wall

3 Validation of Engine Motoring Simulation Gas Exchange Process

The first step in simulating the in-cylinder flow field is to accurately model the gas exchange process. An accurate modeling of the gas exchange process should provide similar profile between the experimental motoring pressure trace and the simulation pressure trace. This comparison is presented in Fig. 3. The experimental and simulated motoring pressures are well correlated for all mass air flow rates.

The mass air flow rates (MAF) of up to 4.8 g/s are achieved under normally aspirated conditions with gradual opening of the throttle. Thereafter, the throttle position is kept constant, and the boost pressure is increased gradually to increase the MAF to 15.1 g/s. Table 3 summarizes the validation conditions and lists the error

Table 3. Validation conditions and errors

MAF [g/s]	p_{int} [kPa gauge]	Δp_{max_err} [%]	MAF [g/s]	p_{int} [kPa gauge]	Δp_{max_err}
3.05	0	−0.02	**7.40**	40	1.30%
4.20	0	−0.29	**10.00**	80	1.78%
4.80	0	−0.24	**15.10**	95	0.49%

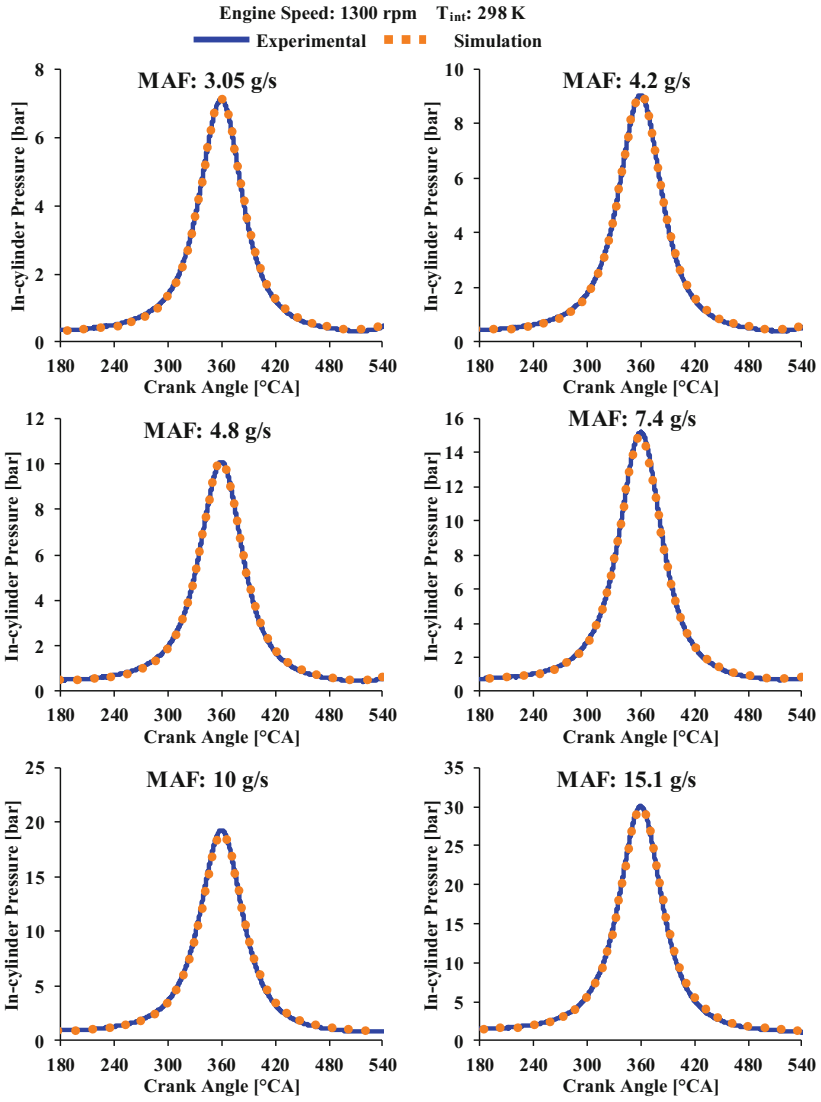

Fig. 3. In-cylinder pressure validation at different mass air flow rates

between the experimental and simulated maximum pressure (denoted by Δp_{max_err}), calculated using Eq. (1) (expressed as percentage). All errors were below 2%.

$$\Delta p_{\max\_err} = \left(p_{\max\_exp} - p_{\max\_sim}\right)/p_{\max\_exp} \tag{1}$$

where p_{max_exp} and p_{max_sim} refer to the experimental and simulated maximum in-cylinder pressures, respectively.

4 Results and Discussion

This section is divided into two subsections. The first subsection describes the results of the cross-flow simulation. The second subsection describes the results of the engine motoring simulation.

4.1 Steady and Uniform Cross-Flow Simulation

The steady cross-flow simulation is performed at inflow velocities of 10, 20, 40, and 100 m/s. The flow conditions in the spark gap are expected to affect the initial breakdown and spark kernel formation. Therefore, the average values of turbulent velocity and turbulence intensity are calculated in the spark gap over a cylindrical volume which is 0.9 mm in diameter and 0.77 mm in height bringing the total volume to approximately 0.5 mm^3.

Figure 4 shows the turbulent velocity and the turbulence intensity in the gap. Turbulent velocity "u'" is defined as the root mean square value of the fluctuating velocity components. Mathematically, it is calculated from the turbulent kinetic energy using expression given by Eq. (2) [23].

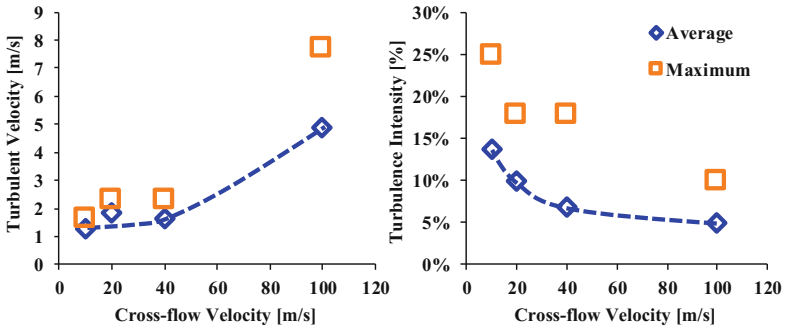

Fig. 4. Steady cross-flow – fluctuating velocity (left) and turbulent intensity (right)

$$u' = \sqrt{\frac{2}{3}k} \tag{2}$$

where "k" represents the turbulent kinetic energy of the flow. Turbulence intensity "I" is the ratio of turbulent velocity to the mean flow velocity magnitude "$\overline{U}$" and is given by Eq. (3).

$$I = \frac{u'}{\overline{U}} \tag{3}$$

Figure 4 shows the results of spark test under steady cross-flow of air on the spark gap. The maximum values are also shown for each inflow condition (square markers) to

highlight the variation in the measurement volume. The turbulent velocity (calculated from the root mean square of the fluctuating velocity) increases with increasing inflow velocity. The spark plug electrodes act like bluff bodies in the flow, generating turbulence in their wake. The variation in turbulent velocity in the spark gap is limited at low inflow velocities but this variation increases at the highest inflow velocity of 100 m/s. However, given the small dimensions of the electrodes and the gap itself, the turbulent velocity does not increase at the same rate as the mean stream velocity when the inflow velocity increases. Therefore, the turbulence intensity shows a decreasing trend with increasing inflow velocity.

At no flow condition, after the spark breakdown, a steady arc can be maintained between the two electrodes [21]. However, with increase in the cross-flow velocity, the arc stretches until it breaks and must be re-established, which leads to the oscillations in the current signal as shown in Fig. 5, left. The frequency of the re-establishment of this plasma channel is termed as the restrike frequency. The restrike frequency increases with increase in the cross-flow velocity as shown in Fig. 5 right. Figure 6 shows the simulation results for the turbulent velocity (left) and the vorticity (right) in the form of contour plots at three different cross-flow velocities of 10, 40, and 100 m/s. The turbulent velocity predicted downstream of the spark plug is probably due to the bluff body effect. The center of the spark gap typically has no turbulence, but the turbulence around the electrodes may affect the plasma channel. The recirculation zone downstream of the gap increases in area with increasing cross-flow velocity. Again, the range of turbulent velocity also increases with increasing cross-flow velocity which causes the increase in the turbulent velocity in the gap (Fig. 4). The vector quantity of vorticity can be physically interpreted as the number of rotations of the eddies per unit time. Mathematically, vorticity represents the curl of the velocity vector. The tensor form of vorticity calculations is given by Eq. (4) [23].

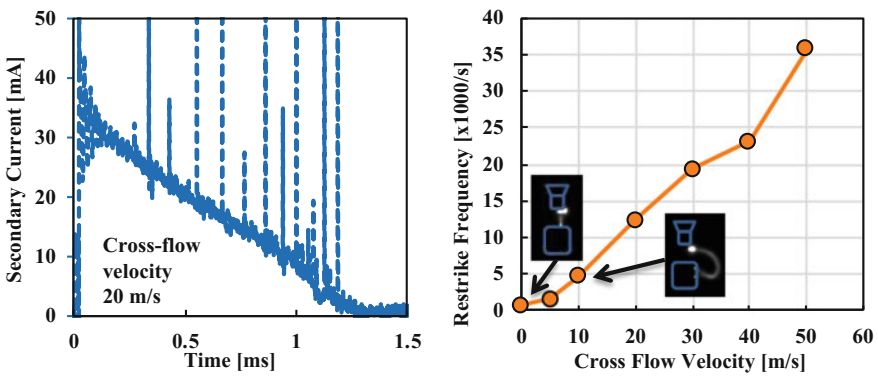

Fig. 5. Spark test – secondary current for 20 m/s cross-flow velocity (left) and restrike frequency (right) [21]

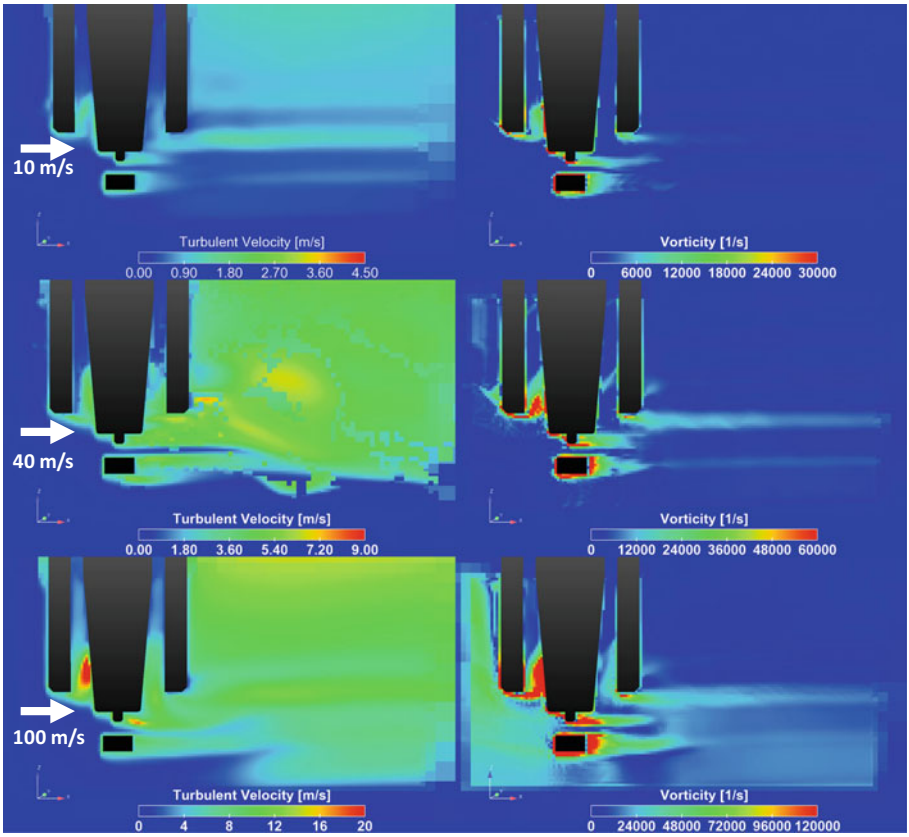

Fig. 6. Steady cross-flow at 10, 40, 100 m/s – turbulent velocity (left) and vorticity (right)

$$\omega = \nabla \times \bar{u} = \left(\frac{\partial u_k}{\partial x_j} - \frac{\partial u_j}{\partial x_k}\right)\hat{\imath} - \left(\frac{\partial u_k}{\partial x_i} - \frac{\partial u_i}{\partial x_k}\right)\hat{\jmath} - \left(\frac{\partial u_j}{\partial x_i} - \frac{\partial u_i}{\partial x_j}\right)\hat{k} \tag{4}$$

where u_i, u_j, and u_k are the x, y, and z components of the velocity, respectively.

As illustrated in the contour plots, the vorticity increases with increasing cross-flow velocity. Vorticity and restrike frequency follow a similar increasing trend with increasing the cross-flow velocity. At 10 m/s and 40 m/s cross-flow velocities, the vorticities are in the range of 6000–12000 s^{-1} and 24000–36000 s^{-1}, which seems to correlate with the restrike frequencies of the spark discharge (Fig. 5) at these cross-flow velocities (5000 s^{-1} and 24000 s^{-1}, respectively). The cross-flow simulation study gives an estimation of the influence of the spark plug geometry in generating turbulence in its wake.

4.2 Engine Motoring Simulation

In this subsection, the results for simulation of one gas exchange cycle of the engine are described. A cycle is described from 0 to 720 °CA with the compression TDC at 360 ° CA. Increasing the mass air flow (MAF) of the engine while maintaining the same fuel injection quantity would make the fuel–air mixture leaner. Two types of methods to increase the MAF into the engine are studied—increasing the throttle opening and increasing intake pressure at a constant throttle opening. The typical spark timing window of 300 to 360 °CA is investigated.

Since the focus of this research is the flow field around the spark plug, two planes are selected for analysis which pass through the electrode gap denoted by the cross-flow plane and the J-plane (illustrated in Fig. 7). Similar to the steady cross-flow analysis, the average of the magnitudes of velocity and root mean square velocity, and the turbulence intensity are calculated in the spark gap over a cylindrical volume which is 0.9 mm in diameter and 0.77 mm in height bringing the total volume to approximately 0.5 mm^3. This gap averaging volume is highlighted in Fig. 7. Similar to the validation conditions, the engine speed and intake temperature are constant.

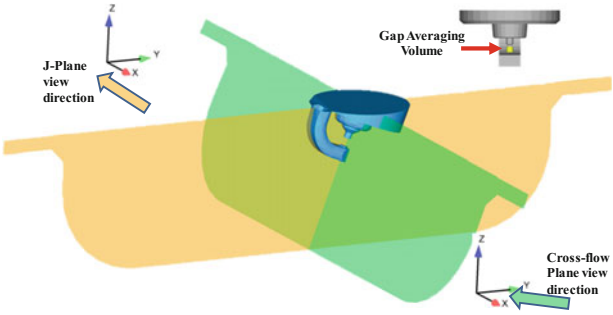

Fig. 7. Result analysis planes and gap averaging volume

4.2.1 Increasing Throttle Opening

During the engine test, the throttle is opened gradually to increase the MAF from 3.05 to 4.8 g/s under normally aspirated intake condition. The corresponding manifold pressure profiles are used as the boundary conditions for the inflow boundary in the simulations. In this MAF range, there is no significant difference in the calculated magnitude of the flow velocity in the spark gap (Fig. 8, left). The overall flow velocity magnitude is highest between 310 to 320 °CA and shows a decreasing trend as the piston approaches TDC.

The turbulence intensity increases since the gap velocity magnitude decreases (plotted with round markers in Fig. 8, right) but the turbulent velocity magnitude remains in the range of $\sim$1 m/s. The turbulent kinetic energy (TKE) decreases since it is a function of the gap velocity (plotted with square markers in Fig. 8, right). Again, the two MAF levels show similar results. Figure 9 shows plots of the maximum velocity magnitudes on each of the analyses planes in the gap. The maximum velocity

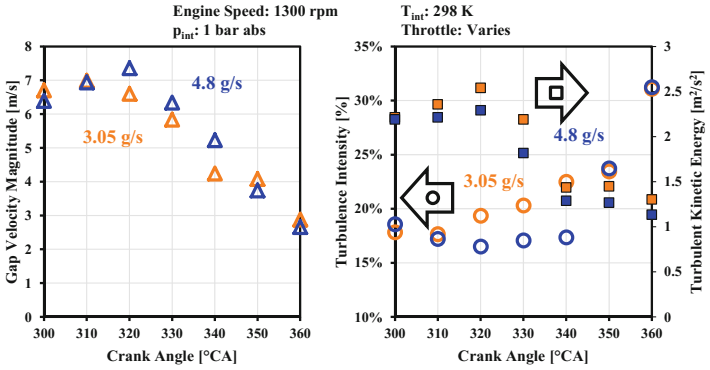

Fig. 8. Throttle opening increase – gap velocity magnitude (left) and turbulence intensity and TKE (right)

in the cross-flow plane is estimated to be between 315 and 330 °CA, and the trends of velocity are similar at the three MAF levels. The velocity in the J-plane reaches a minimum magnitude between 325 and 335 °CA. The velocities in the J-plane for the 4.2 and 4.8 g/s MAF cases are similar, but the velocity is highest in the 3.05 g/s case.

In order to interpret these results, a detailed study of the flow field in the vicinity of the spark plug is required. The velocity and the vorticity contours are shown in Figs. 10 and 11, respectively, in the cross-flow plane over the 310–360 °CA range for the 4.8 g/s MAF case. The velocity vectors are also shown in Fig. 10. Between 310 and 340 °CA, the flow in the gap is directed from −X to +X direction (coordinate system in Fig. 7). Thereafter, the flow direction begins to switch which can explain the local minima in the maximum cross-flow velocity magnitude in the gap (Fig. 9, left). The flow field in the cylinder is affected by both the geometry of the intake port and the geometry of the combustion chamber. As the piston reaches TDC toward the end of the compression stroke, the squish effect can cause a change in the global air motion in the

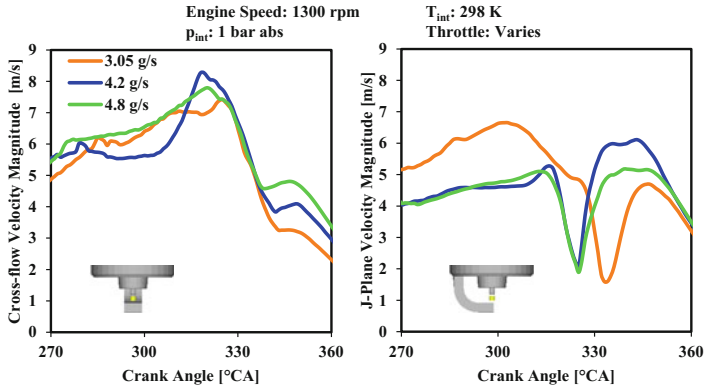

Fig. 9. Maximum velocity magnitude in the analysis planes

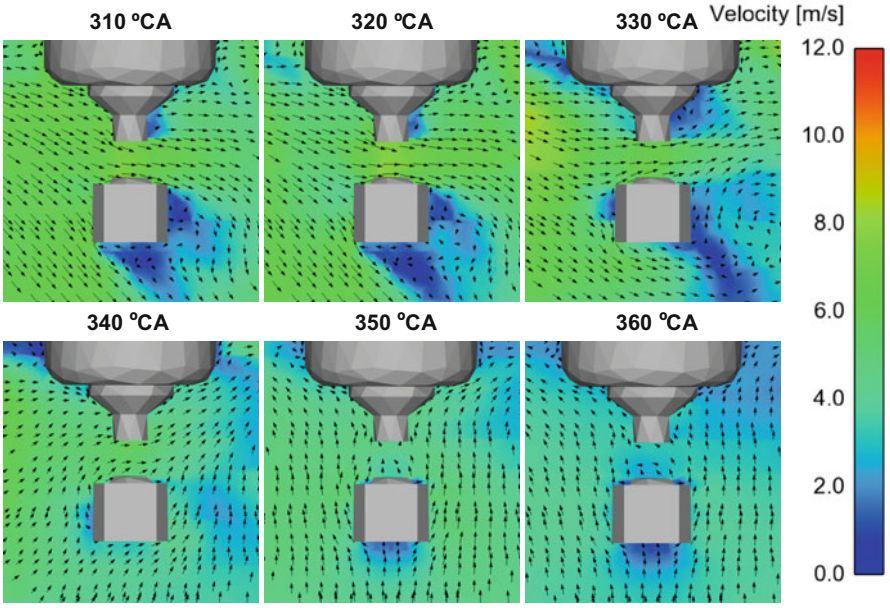

Fig. 10. Velocity contours with vector arrows in the cross-flow plane for MAF of 4.8 g/s

cylinder which in turn can cause the switch in the flow direction through the gap. There is a recirculation zone formed downstream of the ground electrode which is most evident at 330 °CA. The vorticity magnitude in this zone and in the gap is in the range of 6000–8000 s^{-1}, which is similar to the steady cross-flow vorticity results for ~8–10 m/s cross-flow velocity (Fig. 11). The vorticity decreases as the piston approaches TDC. This would imply that some of the best conditions for sustaining the arc would be closer to the TDC after 340 °CA. However, in the case of lean combustion, the spark timing typically has to be advanced to provide sufficient time for the combustion to complete. Therefore, it may be required to initiate and sustain ignition under high flow conditions.

Figure 12 shows the velocity and vorticity contours in the J-plane for the 4.8 g/s MAF case. Analogous to the cross-flow plane, the bulk flow direction changes from outward of the ground electrode to heading toward the ground electrode at 350 °CA. Again, this indicates a switch in the bulk in-cylinder gas motion. There are two recirculation zones in the −Y and the +Y direction (global coordinates in Fig. 7) on both sides of the central electrode with vorticities in the range of 6000–8000 s^{-1}. The vorticity decreases as the piston moves closer to TDC. The ground electrode may play a crucial role in the spark kernel formation. It could shield the gap from flow effects during the initial stage of the spark discharge, and later may hinder the flame propagation as the flame kernel ignites the remainder of the fuel–air mixture. Under this particular operating condition and for this engine geometry and spark plug orientation, it would seem more beneficial for the flow to assist the flame in propagating away from

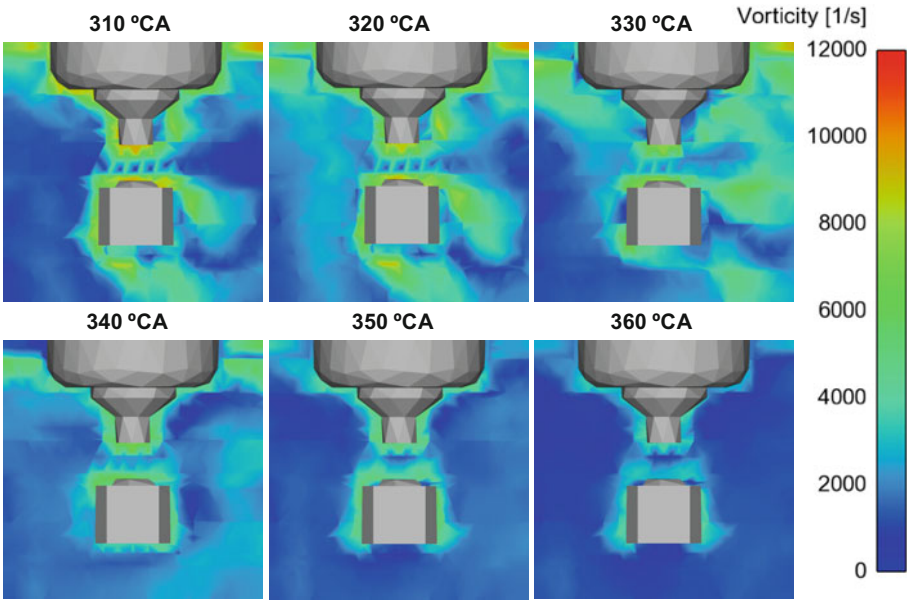

Fig. 11. Vorticity contours in the cross-flow plane for MAF of 4.8 g/s

the ground electrode and into the combustion chamber which may not occur at late spark timings.

4.2.2 Increasing Intake Pressure

The next set of results simulates the engine operating conditions at which the throttle opening is held constant, and the intake pressure is increased to increase the MAF from 7.4 g/s to 15.1 g/s. Again, the manifold pressure profile is used as the pressure boundary condition for the inflow boundary. Figure 13, left shows the magnitude of the gap velocity for the 7.4 and 15.1 g/s MAF cases. The trends differ significantly with piston movement. With increasing intake pressure, the gap velocity decreases. The maximum gap velocity in the analysis planes is given in the appendix.

The turbulent intensity and the turbulent kinetic energy are inversely and directly correlated to the gap velocity, respectively (Fig. 13, right). Beyond 330 °CA, the turbulent kinetic energies for 7.4 and 15.1 MAF cases are similar. The increase in intake pressure is expected to enhance the flow in the cylinder due to a higher pressure differential. However, it may not necessarily increase the flow velocity in the spark gap. In fact, increase in intake pressure and consequent increase in the MAF increase the overall in-cylinder swirl ratio and tumble ratio (shown in Fig. 14). The 3.05 g/s MAF case is also shown for reference. Due to the orientation of the spark plug (Fig. 7), the gap velocity is affected primarily by the swirl motion and the tumble across Y-axis. Flow is shielded by the ground electrode in the X-axis tumble plane. Swirl ratio during the suction stroke increases with an increase in intake MAF, but this swirl motion is not sustained through the compression stroke and the trend is inverted near the spark

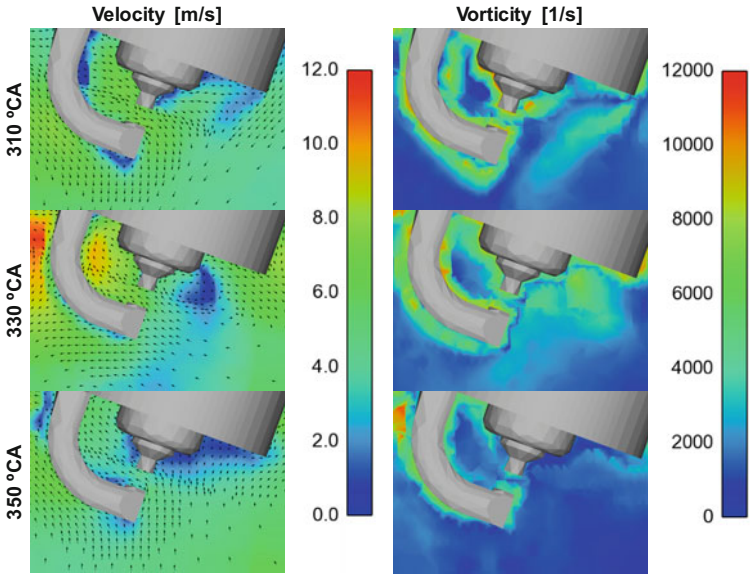

Fig. 12. Velocity and vorticity contours in the J- plane for MAF of 4.8 g/s

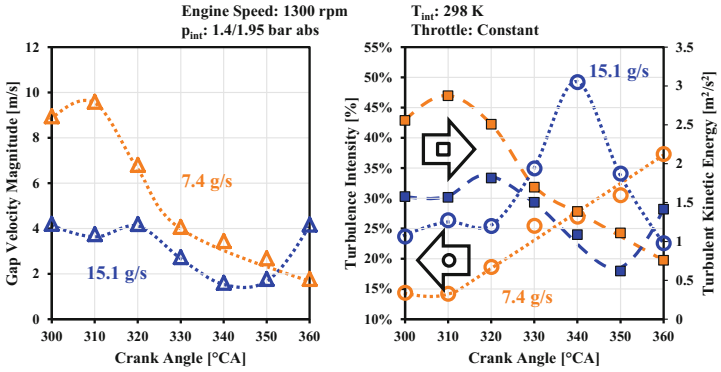

Fig. 13. Intake pressure increase – gap velocity magnitude (left) and turbulence intensity and TKE (right)

timing window. MAF seems to have negligible effect on the tumble around Y-axis near the spark timing window. This reduction in intensity of swirl motion near the spark window can contribute toward reduced flow velocity magnitude in spark gap. Additionally, a reversal in cross-flow direction can be observed near TDC (shown in Fig. 15), which may be a consequence of the change in overall in-cylinder flow field. This implies that the flow in the spark gap can reduce even when the bulk gas velocity is boosted.

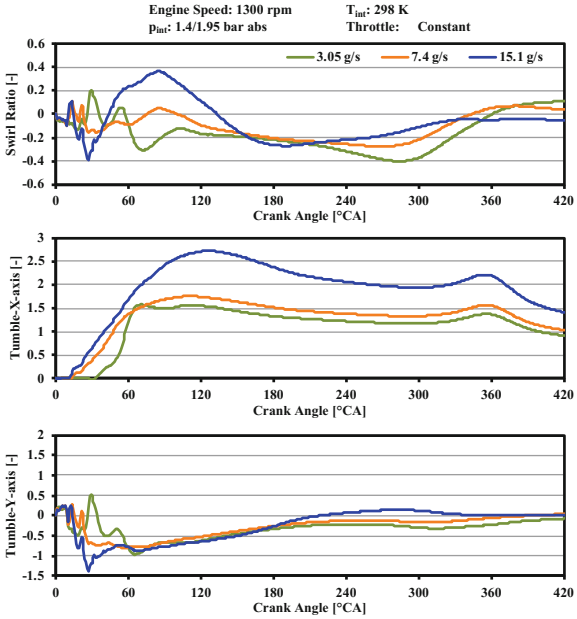

Fig. 14. Intake pressure increase – swirl ratio and tumble ratio across the X- and Y-axes

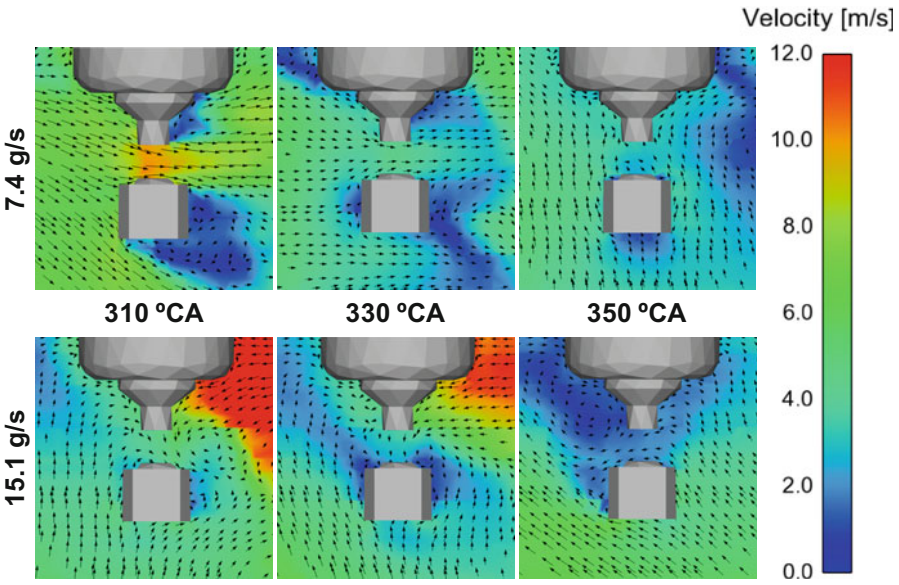

Fig. 15. Velocity contours with vector arrows in the cross-flow plane for MAF of 7.4 and 15.1 g/s

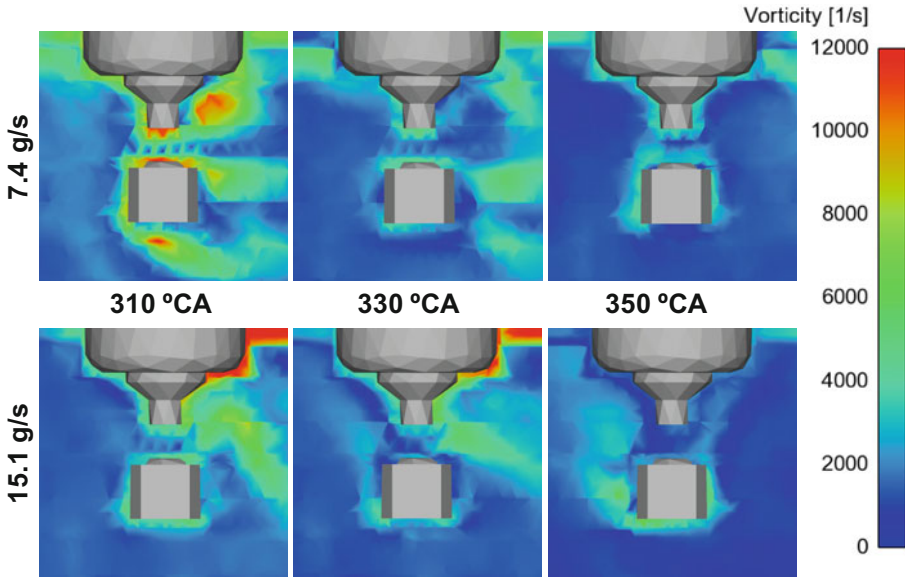

Fig. 16. Vorticity contours in the cross-flow plane for MAF of 7.4 and 15.1 g/s

Figure 15 illustrates a comparison of the velocity contours at the two MAF cases along with the velocity vectors in the cross-flow plane. The flow field around the spark plug on the cross-flow plane is distinct for each case. For the 7.4 g/s case, the flow direction changes beyond 330 °CA possibly due to the change in the flow direction of the bulk gas. The swirl ratio also changes sign at the same crank position (Fig. 14) for the 7.4 g/s case. Moreover, there is the formation of a recirculation zone downstream of the ground electrode. Highest vorticity magnitude in the gap is calculated at 310 °CA. The vorticity in this case is again in the range of 6000–8000 s^{-1} and reduces subsequently as the turbulence decays.

The peak velocity of $\sim$10 m/s is determined at 310 °CA and reduces as the piston moves toward the TDC (Fig. 15). For the 15.1 g/s case, the flow field is much more dynamic. However, the gas flow velocity in the gap never exceeds 5 m/s in the 300 to 360 °CA range. Higher velocity regions (>12 m/s) can be seen near the spark plug which indicates that the bulk gas velocity may be higher than the gap flow velocity. Various recirculation zones are also predicted near the electrodes with vorticity in most of the regions in the range of 6000–8000 s^{-1} (Fig. 16). Maximum vorticity around the gap can reach 8000–10000 s^{-1}. Vorticity reduces as TDC is approached. For this particular engine configuration and operating conditions, with increasing pressure, the flow velocity in the spark gap reduces.

In the J-plane, the vorticity of the recirculation zones around the electrodes is higher for the 15.1 g/s case compared to the 7.4 g/s case (Fig. 17). The vorticity magnitude in the gap on the J-plane for the 15.1 g/s case is lower than the 7.4 g/s case and is in accordance with the reduced flow strength in the spark gap with increasing pressure.

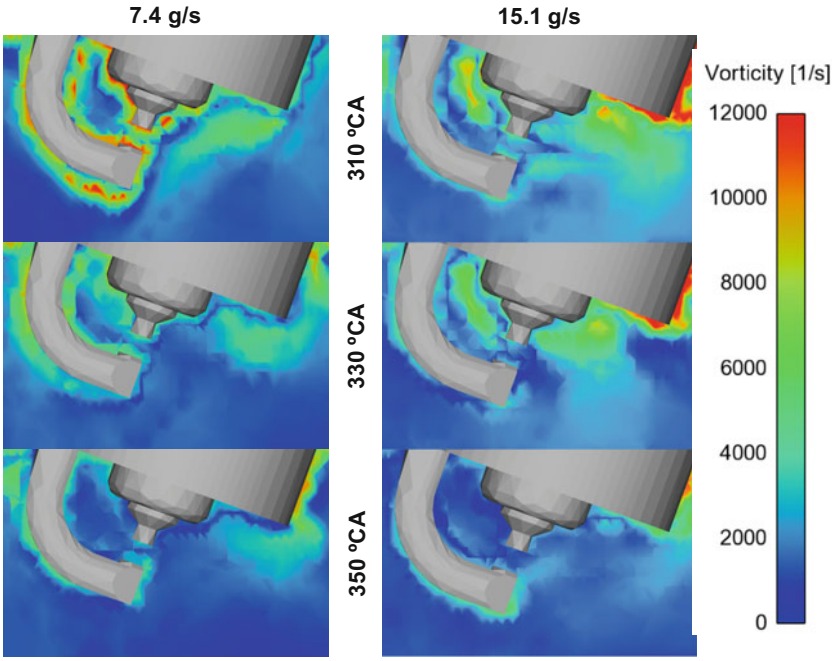

Fig. 17. Vorticity contours in the J-plane for MAF of 7.4 and 15.1 g/s

Detailed empirical studies of the in-cylinder flow field are required to validate the simulation results. Such studies typically require engines with optical access. An indirect method could be analysis of the spark current profile since a relationship between the empirical spark restrike frequency and the simulated vorticity is observed in this study.

5 Summary

The authors performed CFD analysis of the flow fields around a spark plug under steady and uniform flow, and under engine motoring conditions. Motoring simulations were performed with increasing MAF. Two methods to increase the intake MAF were studied—opening throttle and increasing intake pressure. These simulations utilized the empirical intake manifold pressure profile as the inflow boundary condition. The engine motoring simulation cases were validated with engine pressure data to ensure that the gas exchange process was accurately modeled. The main conclusions of this CFD study are as follows:

- Under steady and uniform cross-flow, the spark plug acts like a bluff body, and turbulence is generated in the wake of the plug.

- The vorticity of the eddies which are created in the wake of the spark plug cross-flow is of the same order as the frequencies of the arc restrike in empirical study of the spark discharge with cross-flow.
- There are no significant differences in the flow profiles with increasing throttle opening over the MAF range studied. The gap velocity and turbulent kinetic energy decrease as the piston approaches TDC. The gap velocity direction is also switched near TDC. Different recirculation zones are identified with vorticity magnitudes similar to the steady cross-flow cases.
- When the intake pressure is increased to increase the MAF, there are major differences in the flow field between different MAF cases. The gap velocity decreases with increasing MAF. The bulk gas flow velocity increases with increasing MAF but it may not increase the flow speed in the spark gap.
- The gap velocity and the turbulent kinetic energy in the gap decrease as the piston approaches TDC.
- The vorticity of the flow field around the spark gap is higher for the highest pressure case in comparison to the lowest pressure case.

Acknowledgements. The authors gratefully acknowledge Convergent Science for the use of their simulation suite (version 2.3) and ANSYS for the use of EnSight (version 10.1). Furthermore, the authors acknowledge the Canada Research Chair program, NSERC, CFI, OIT, the University of Windsor, Ford Motor Company, and other OEMs for their support of the research at the Clean Combustion Engine Laboratory.

Nomenclature

AMR	Adaptive Mesh Refinement
BTDC	Before Top Dead Center
CFD	Computational Fluid Dynamics
DC	Direct Current
EGR	Exhaust Gas Recirculation
IC	Internal Combustion
k	Turbulent kinetic energy
MAF	Mass Air Flow
NOx	Nitrogen Oxides
RNG	Renormalized Group
SI	Spark Ignition
TDC	Top Dead center
$\overline{U}$	Mean flow velocity
u’	Turbulent velocity
ε	Dissipation Rate
ω	Vorticity

Appendix: Maximum Velocity Magnitude in the Analysis Planes with Increasing Intake Pressure

See Fig. 18.

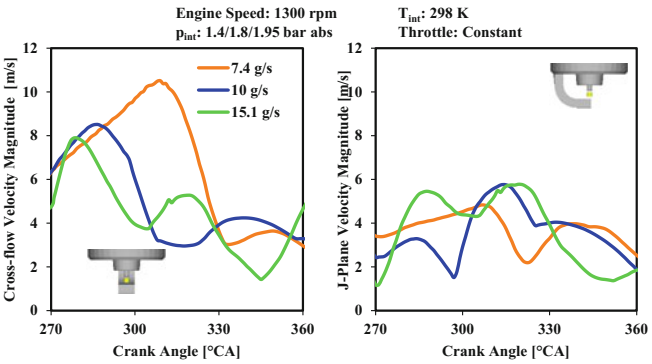

Fig. 18. Maximum velocity magnitude in analysis planes with increasing intake pressure

References

1. National Research Council: Transitions to Alternative Vehicles and Fuels. The National Academies Press, Washington, DC (2013)
2. National Research Council: Review of the Research Program of the FreedomCAR and Fuel Partnership: Third Report. The National Academies Press, Washington, DC (2010)
3. Hsieh, W.-D., Chen, R.-H., Wu, T.-L., Lin, T.-H.: Engine performance and pollutant emission of an SI engine using ethanol–gasoline blended fuels. Atmos. Environ. **36**, 403–410 (2002)
4. Yang, Z., Bandivadekar, A.: 2017 global update: light-duty vehicle greenhouse gas and fuel economy standards. The International Council on Clean Transportation (2017). https://www.theicct.org/publications/2017-global-update-LDV-GHG-FE-standards. Accessed 11 May 2018
5. Germane, G.J., Wood, C.G., Hess, C.C.: Lean combustion in spark-ignited internal combustion engines-a review. SAE Technical Paper 831694 (1983)
6. Attard, W.P., Blaxill, H.: A lean burn gasoline fueled pre-chamber jet ignition combustion system achieving high efficiency and low NOx at part load. SAE Technical Paper 2012-01-1146 (2012)
7. Wei, H., Zhu, T., Shu, G., Tan, L., Wang, Y.: Gasoline engine exhaust gas recirculation–a review. Appl. Energy **99**, 534–544 (2012)
8. Diana, S., Giglio, V., Iorio, B., Police, G.: A strategy to improve the efficiency of stoichiometric spark ignition engines. SAE Technical Paper 961953 (1996)
9. Takahashi, D., Nakata, K., Yoshihara, Y., Ohta, Y., Nishiura, H.: Combustion development to achieve engine thermal efficiency of 40% for hybrid vehicles. SAE Technical Paper 2015-01-1254 (2015)

10. Nakata, K., Nogawa, S., Takahashi, D., Yoshihara, Y., Kumagai, A., Suzuki, T.: Engine technologies for achieving 45% thermal efficiency of S.I. Engine. SAE Int. J. Engines **9**, 179–192 (2016)
11. Kuo, T.-W.: What causes slower flame propagation in the lean-combustion engine? J. Eng. Gas Turbines Power **112**, 348–356 (1990)
12. Arcoumanis, C., Whitelaw, J.H.: Fluid mechanics of internal combustion engines—a review. Proc. Instit. Mech. Eng. Part C: J. Mech. Eng. Sci. **201**, 57–74 (1987)
13. Ives, M.E.: Enhancement of intake generated swirl to improve lean combustion. MASc thesis, Electronic Theses and Dissertations. University of Windsor, Windsor, ON, Canada (2017)
14. Ozdor, N., Dulger, M., Sher, E.: Cyclic variability in spark ignition engines a literature survey. SAE Technical Paper 940987 (1994)
15. Shen, H., Hinze, P.C., Heywood, J.B.: A model for flame initiation and early development in si engine and its application to cycle-to-cycle variations. SAE Technical Paper 942049 (1994)
16. Johansson, B.: Cycle to cycle variations in S.I. Engines-the effects of fluid flow and gas composition in the vicinity of the spark plug on early combustion. SAE Technical Paper 962084 (1996)
17. Sayama, S., Kinoshita, M., Mandokoro, Y., Fuyuto, T.: Spark ignition and early flame development of lean mixtures under high-velocity flow conditions: an experimental study. Int. J. Engine Res. (2018). https://doi.org/10.1177/1468087417748517
18. Aleiferis, P.G., Taylor, A.M.K.P., Whitelaw, J.H., Ishii, K., Urata, Y.: Cyclic variations of initial flame kernel growth in a honda VTEC-E lean-burn spark-ignition engine. SAE Technical Paper 2000-01-1207 (2000)
19. Arcoumanis, C., Bae, C.-S.: Visualization of flow/flame interaction in a constant-volume combustion chamber. SAE Technical Paper 930868 (1993)
20. Ballal, D.R., Lefebvre, A.H.: The influence of spark discharge characteristics on minimum ignition energy in flowing gases. Combust. Flame **24**, 99–108 (1975)
21. Yu, X., Yang, Z., Yu, S., Ives, M., Zheng, M.: Discharge characteristics of current boosted spark events under flow conditions. In: ASME Internal Combustion Engine Division Fall Technical Conference, 15–18 October 2017, pp. V001T03A017 (2017)
22. Schneider, A., Leick, P., Hettinger, A., Rottengruber, H.: Experimental studies on spark stability in an optical combustion vessel under flowing condition. In: Liebl, J., Beidl, C. (eds.) Internationaler Motorenkongress 2016, pp. 327–348. Springer Fachmedien Wiesbaden (2016)
23. ConvergeCFD, ConvergeCFD Manual Series–Converge 2.3 Manual, Convergent Science (2016)